Accepted to ApJ

Comparative Lyot Coronagraphy with Extreme AO Systems

Justin R. Crepp, Andrew D. Vanden Heuvel, & Jian Ge

Astronomy Department, University of Florida
211 Bryant Space Science Center, P.O. Box 112055
Gainesville, FL 32611-2055

jcrepp@astro.ufl.edu, avheuv@gmail.com, jge@astro.ufl.edu

ABSTRACT

As adaptive optics technology continues to improve, the stellar coronagraph will play an ever increasing role in ground-based high-contrast imaging observations. Though several different image masks exist for the most common type of coronagraph, the Lyot coronagraph, it is not yet clear what level of wavefront correction must be reached in order to gain, either in starlight suppression or observing efficiency, by implementing a more sophisticated design. In this paper, we model image plane Lyot-style coronagraphs and test their response to a range of wavefront correction levels, in order to identify regimes of atmospheric compensation where the use of hard-edge, Gaussian, and band-limited image masks becomes observationally advantageous. To delineate performances, we calculate the speckle noise floor mean intensity. We find that apodized masks provide little improvement over hard-edge masks until on-sky Strehl ratios exceed $\sim 0.88\, S_{qs}$, where S_{qs} is the intrinsic Strehl ratio provided by the optical system. Above this value, 4th-order band-limited masks out-perform Gaussian masks by generating comparable contrast with higher Lyot stop throughput. Below this level of correction, hard-edge masks may be preferentially chosen, since they are less susceptible to low-order aberration content. The use of higher-order band-limited masks is relegated to situations where quasi-static residual starlight cannot be sufficiently removed from the search area with speckle-nulling hardware.

Subject headings: stars: imaging — atmospheric effects — instrumentation: adaptive optics, high angular resolution — methods: numerical

1. INTRODUCTION

In recent years, great strides in the development of adaptive optics (AO) technology have ushered in a new era of high resolution diffraction-limited imaging. Despite these advances, the ability of the stellar coronagraph to generate deep contrast remains limited by insufficient levels of wavefront control; uncorrected phase and amplitude errors induced by the atmosphere and instrument optics manifest as bright, dynamic 'speckles' of scattered light in the search area. Even the most basic coronagraph, a Lyot coronagraph equipped with a focal plane hard-edge occulter (Lyot 1939), is incapable of reaching its peak performance when coupled to state-of-the-art AO (Oppenheimer 2004).

Numerous high-contrast observations have been conducted using AO on the world's largest telescopes (Marois et al. 2006, Mayama et al. 2006, Itoh, Oasa, & Fukagawa 2006, Carson et al. 2005a, Close et al. 2005, Metchev & Hillenbrand 2004, Debes et al. 2002, Liu et al. 2002, and references therein); some rely solely on AO imaging, while others combine AO with coronagraphy[1] and/or speckle reduction techniques. These efforts have provided the first image of a candidate extrasolar planet (Chauvin et al. 2004), as well as direct detections of sub-stellar companions near the planet-brown dwarf boundary (Biller et al. 2006, Neuhäuser et al. 2005, Chauvin et al. 2005). However, to image older, less-massive, and closer-in planets from the ground, wavefront sensing and correction techniques must improve substantially.

"Extreme" advances in high-contrast imaging technology are anticipated in the coming years. Deformable mirrors employing several thousand actuators and wavefront sensing of laser guide stars can, in principle, drive Strehl ratios above 90% on 8-10m class telescopes. With the proper coronagraph, these systems will be capable of detecting the near-IR emission of Jovian planets over a broader range of ages, masses, and separations (see Macintosh et al. 2003). Extremely large telescopes such as the proposed Thirty Meter Telescope (TMT; Macintosh et al. 2006, Troy et al. 2006, Ellerbroek et al. 2005) and 100m OverWhelmingly Large telescope (OWL; Brunetto et al. 2004) will improve spatial resolution, and hence the inner-working-angle (hereafter IWA) on the sky.

An interesting and more immediate alternative, which uses current AO technology, can also provide highly corrected wavefronts by instead sacrificing spatial resolution in return for improved pupil sampling. Serabyn et al. 2007 have demonstrated K-band Strehl ratios approaching 94% by reimaging a 1.5m diameter circular unobstructed subaperture of the

[1]Interferometers are likewise capable of suppressing starlight, and generally have a better inner-working-angle but a more restricted search area (Absil et al. 2006, Serabyn et al. 2005).

Hale 200-inch telescope onto the existing deformable mirror via relay optics. Combining this technique with a coronagraph that has an intrinsically small IWA ($< 3\,\lambda/D$) shows promise for generating deep contrast for separations as close as ~ 0.5".

These considerations motivate the need for a quantitative understanding of how the stellar coronagraph's utility will depend on future gains in AO proficiency. To address this topic, we have modeled systems that are equipped with a variety of amplitude image masks, and examined their performance in a broad, nearly continuous range of corrected wavefront levels. With this paper, we seek to provide a concise guide to the use of Lyot-style image plane coronagraphs. Most notably, we answer the question: "What is the appropriate choice of image mask for an extreme AO system operating at a given Strehl ratio?".

Before proceeding however it is important to discuss an impediment that currently burdens all of the observational surveys listed above. In the next section, we describe quasi-static aberrations and the potential to suppress them to levels sufficient for direct substellar companion detection. The topical outline for the remainder of the paper consists of our numerical techniques, results, and summary and concluding remarks, which are discussed in §3, §4, and §5 respectively.

2. Quasi-Static Aberrations

In addition to atmospheric turbulence, perturbations to the optical path likewise occur once starlight reaches the telescope and instrument optics. Of considerable concern are errors introduced downstream from the AO deformable mirror (DM) and wavefront sensor. The effects of these more systematic disturbances manifest as slowly undulating, quasi-static speckles in the image plane that change on a timescale commensurate with the telescope tracking, thermal fluctuations, and/or other flexures to the opto-mechanical system. Such aberrations are inherent to all instruments and unavoidable at the contrast levels required for circumstellar science.

Speckle-nulling is the act of removing quasi-static residual starlight from a pre-selected region of the image plane. By including one or more additional DMs in the optical train pupil planes to reshape the phase of starlight, a sharply defined region of deeper contrast can be generated over a fraction of the search area. The size of this so-called "dark hole" is governed by the number of extra DMs and their actuator densities. This technique greatly improves the chances for direct detection by properly isolating the companion's mutually incoherent signal. Laboratory results from the High Contrast Imaging Testbed (HCIT; Trauger et al. 2004, Borde et al. 2006) have shown that speckle-nulling is indeed quite feasible down to the

contrast levels potentially accessible to ground-based coronagraphs. High-contrast imaging systems should be equipped with such capabilities, since explicit removal of scattered light with hardware will yield the most unambiguous sub-stellar companion detections and spectra.

Differential imaging techniques such as Simultaneous Differential Imaging (SDI; Racine et al. 1999, Marois et al. 2005, Close et al. 2005, Biller et al. 2006), Angular Differential Imaging (ADI; Marois et al. 2006), and others (see Guyon 2004 and references within) can also help to circumvent the problem of quasi-static aberrations. For example, by subtracting images taken simultaneously in different, carefully chosen bandpasses (SDI) or subsequently at different roll-angles (ADI), it is possible to enhance the effective contrast and detect companions whose brightness falls below the speckle noise floor. These techniques are quite powerful and can even be used in concert. They are limited only by the standard deviation of the stellar residual signal.

In the following, we compare image mask performances by calculating the direct output of the coronagraph, i.e. the mean intensity, with the understanding that differential and post-processing techniques can always be used on top of direct imaging to improve the prospects for discovery.

3. NUMERICAL SIMULATIONS

The theoretical model used for our simulations consists of an extreme AO system linked in series to a Lyot coronagraph that is observing a stellar point source. Wavefront correction levels spanning from not quite diffraction limited ($\sim 77\%$ Strehl) to highly corrected ($\sim 96\%$ Strehl) are generated with an IDL routine based on simulations described in Carson et al. 2005b. The code is optimized to simulate the operation of PHARO (Hayward et al. 2001) with the PALAO system (Troy et al. 2000) on the Hale 200-inch telescope at Palomar.

To clearly elucidate the sometimes subtle differences in performance between coronagraphic image masks, we restrict our analysis to monochromatic light ($\lambda = 2.2\,\mu m$), and ignore the effects of central obstructions, their support structures, and inter-segment mirror gaps. To first order, the addition of each of these complexities can be understood by convolving the telescope entrance aperture with the spatial frequency spectrum of the mask, and observing the resultant light distribution in the Lyot plane. The net effect is often simply a loss in off-axis throughput, as the Lyot stop size is necessarily reduced to reject the additional diffracted starlight. Abe et al. 2006, Sivaramakrishnan & Yaitskova 2005, Sivaramakrishnan & Lloyd 2005, Soummer 2005, and Murakami & Baba 2005 discuss the prospects for Lyot coronagraphy with non-trivial entrance aperture geometries. We use a circular unobstructed

entrance aperture, radial image mask, and (hence) a circular Lyot stop.

Kolmogorov phase screens mimic the effects of atmospheric turbulence, where a fixed Fried parameter of 20 cm at 2.0 microns, which has previously been found to best match actual PHARO data (Carson et al. 2005b), is used throughout. To emulate AO correction, the phase screens are Fourier transformed, multiplied by a parabolic high-pass filter (Sivaramakrishnan et al 2001, Makidon et al. 2005), and then inverse-transformed. Improving the degree of wavefront correction is accomplished by increasing the actuator density, which, in turn, raises the critical frequency of the high-pass spatial filter. The linear number of actuators across the pupil ranges from 35 to 94 (962 to 6939 total actuators); in terms of root-mean-square (rms) residual error, this provides a range in correction from $\lambda/13$ to $\lambda/30$.

The resulting AO-corrected wavefronts are then sent to a separate MATLAB coronagraph code for analysis, where the starlight passes through a series of consecutive pupil and image planes. We assume idealized interactions with the optical elements and the image mask (i.e. no scattered light, dust, fabrication errors, ... etc.), and use scalar diffraction theory to calculate the propagation of the electric field. The telescope pupil is constructed as a perfect disk of unit transmission and diameter 512 pixels placed at the center of a 3072 x 3072 padding matrix in order to provide sufficient image plane resolution (6 pixels per λ/D). This choice of matrice sizes results in numerical noise levels below 10^{-12} in contrast, which is negligible compared to the physical speckle noise floor set by the AO system.

We do not explicitly simulate speckle-nulling on top of atmospheric correction. Instead, in §4.1 and §4.2, we assert that "the instrument" corrects for quasi-static aberrations down to the noise floor mean intensity set by diffraction and the atmosphere, for a given AO actuator density. Speckle-nulling is discussed in more depth in §4.3. This assumption is justified given the laboratory experiments mentioned in §2 that demonstrate removal of residual starlight to contrast levels below 10^{-9} within the fractional search area; although, in practice more timely methods for finding the optimal shapes of the extra DMs (preferably < 1 minute) will need to be employed.

4. COMPARATIVE LYOT CORONAGRAPHY

Our study focuses on the subclass of Lyot coronagraphs that control diffracted starlight with amplitude image masks - that is, focal-plane masks that do not modulate the phase

of transmitted light in theory.[2] Such masks reside in the focal-plane wheel of many coronagraphs in operation at major observatories. Among the choices of amplitude image masks, band-limited masks (Kuchner & Traub 2002) can perform the best in principle. In the ideal case, they diffract *all* transmitted on-axis starlight into a narrow region surrounding the edges of the Lyot pupil, and leave an area of infinite dynamic range in the center. Moreover, band-limited masks with arbitrarily broad central nulls can also be constructed (Kuchner, Crepp, & Ge 2005), and have been shown to help combat low-spatial-frequency optical aberrations in numerical simulations (Shaklan & Green 2005) and in laboratory experiments (Crepp et al. 2006).

We include a hard-edge mask, a Gaussian mask, and band-limited (hereafter BL) masks with 4th-order (sinc^2), 8th-order (sinc, sinc^3), and 12th-order (sinc, sinc^2, sinc^3) intensity transmission profiles near the optical axis (Figure 1). Each mask is azimuthally symmetric and designed with an IWA$= 4\ \lambda/D$, so as to make fair comparisons. The IWA is defined as the half-width-at-half-maximum of the intensity transmission profile; for these masks, this value differs by less than 1% from the equivalent width, which can also be used as an alternative definition (Aime 2005). The masks are not truncated in the image plane; in practice, it is easy to include enough resolution elements such that this effect does not contribute significantly to the noise floor. Equations describing the masks are shown below. The radial coordinate, r, measures the distance from the optical axis, where $\tilde{r} = r\ D/\lambda$. Constants, which can be derived from Kuchner, Crepp, & Ge 2005, are given to four decimals of precision. The amplitude transmissions, $M(r)$, are:

$$M_{\mathrm{H}}(r) = \mathrm{circ}\,(\tilde{r}/4) \quad (1)$$

$$M_{\mathrm{G}}(r) = 1 - e^{-(\tilde{r}/3.6097)^2}, \quad (2)$$

$$M_{\mathrm{BL}_{4th}}(r) = 1 - \mathrm{sinc}^2(0.4500\ \tilde{r}), \quad (3)$$

$$M_{\mathrm{BL}_{8th}}(r) = 0.9485 + 0.4743\ \mathrm{sinc}(1.4043\ \tilde{r}) - 1.4228\ \mathrm{sinc}^3(0.4681\ \tilde{r}), \quad (4)$$

$$M_{\mathrm{BL}_{12th}}(r) = 0.7526 - 0.9408\ \mathrm{sinc}(1.9006\ \tilde{r}) + 5.2684\ \mathrm{sinc}^2(0.9503\ \tilde{r}) - 5.0802\ \mathrm{sinc}^3(0.6335\ \tilde{r}), \quad (5)$$

where circ $(\tilde{r}/a)$ is a step-function equal to zero for $\tilde{r} \leq a$ and unity elsewhere.

[2]Masks that manipulate the phase of starlight in the image plane generally have better inner-working-angles but poorer broadband performance (Roddier & Roddier 1997 and Rouan et al. 2000); although, fully achromatic designs are being developed (e.g. Mawet et al. 2005). See Guyon et al. 2006 for a review of the myriad of other different coronagraphic designs and how they compare in a space-based application, such as TPF.

To provide intuition for each mask's potential performance, we first present coronagraph simulations using perfect incident wavefronts (Table 1). A qualitative understanding of the coronagraph's functionality can be gleaned by examining the light distribution pattern in the Lyot pupil plane, since the total amount of rejected starlight depends strongly on the Lyot stop size and shape. For hard-edge and Gaussian masks, the contrast is limited by residual diffracted starlight, whereas the combination of a BL mask with a matching Lyot stop can completely remove all on-axis starlight, in this ideal case. This capability is seen in the 4th-, 8th-, and 12th-order BL mask final image plane patterns; they are composed entirely of numerical noise.

"Degeneracies" in contrast can occur however when large phase errors are present. In other words, different masks may generate indistinguishably similar levels of contrast when uncorrected atmospheric scattered starlight, rather than diffracted starlight, is the dominant source of noise. Under these circumstances, throughput, quasi-static aberration sensitivities, and fabrication considerations should more heavily influence the decision for which mask to implement in practice.

In the following sections, image mask performances are quantified in terms of these parameters and as a function of AO system correction. References to both the rms wavefront error (WFE), σ_{AO}, in the pupil plane and resulting Strehl ratio, S_{AO}, in the image plane are made. The relationship $S_{AO} \approx 1 - (2\pi\sigma_{AO})^2$ is valid in the high Strehl regime, and is adopted for our calculations. We begin by comparing hard-edge masks to the class of graded or apodized masks as a whole.

At this point it is convenient to define contrast, $C(r)$, as it will be used throughout the remainder of the text:

$$C(r) = \frac{I(r)}{\hat{I}(0)\,|M(r)|^2}, \tag{6}$$

where $I(r)$ is the intensity at the radial coordinate in the final image, $\hat{I}(0)$ is the peak stellar intensity as would be measured *without* the image mask in the optical train, and $|M(r)|^2$ is the mask intensity transmission. Note that $I(r)$ and $\hat{I}(0)$ are both measured with the Lyot stop in place. This is the non-differential (i.e non-SDI, single roll-angle, ... etc.) contrast.

4.1. Hard-Edge vs. Apodized Image Masks

A stellar coronagraph will begin to noticeably improve contrast relative to standard AO imaging only when a sufficient amount of starlight is concentrated in the Airy pattern central core. This occurs at Strehl ratios as low as 50%; however, substantial gains over a

significant fraction of the search area are not attained until the Strehl ratio exceeds $\sim 80\%$ (Sivaramakrishnan et al. 2001). We seek to identify the required level of wavefront correction above this value where apodized masks begin to out-perform hard-edge masks.[3]

For this comparison, we hold the Lyot stop size fixed at 60% throughput; images from the Lyot Plane column in Table 1 and results from §4.2 help to clarify why this is a useful simulation control. Contrast curves for the hard-edge, Gaussian, and 4th-order BL masks are shown in Figure 2 using several different levels of wavefront correction. For clarity, higher-order BL masks are not included here, but are discussed in the next sections. They provide intermediate levels of contrast, between that of the hard-edge and the 4th-order BL mask.

At $\sim 77\%$ Strehl (rms WFE $= \lambda/13$), the advantage in using the image plane coronagraph is evident only for separations smaller than $\sim 8\ \lambda/D$; this is a result of the limited wavefront correction and reduced aperture stop in the Lyot plane. Moreover, the Gaussian and 4th-order BL masks provide only a factor of ~ 1.6 improvement over the hard-edge occulter at the IWA, and contrast degeneracy sets in at a distance of $\sim 1.5\,\lambda/D$ from there. As AO correction improves, starlight is redistributed from the scattered light halo into the Airy diffraction pattern, the PSF 'shoulder' drops and extends, and the diffracted light limitations of the hard-edge mask are revealed. The sharp edges of the mask prevent further improvements in contrast below $\sim 10^{-4}$ at the IWA, even as Strehl ratios exceed $\sim 88\%$.

The Gaussian and 4th-order BL masks, which more effectively diffract starlight onto the opaque portions of the Lyot stop, are capable of generating contrast levels of $\sim 6 \times 10^{-6}$ at IWA $= 4\ \lambda/D$ with $\sim 94\%$ Strehl. They provide an improvement in contrast at the IWA over the hard-edge mask by factors of approximately 2.7 at $\sim 82\%$ Strehl (rms WFE $= \lambda/15$), 5.1 at $\sim 88\%$ Strehl (rms WFE $= \lambda/18$), and 21.7 at $\sim 94\%$ Strehl (rms WFE $= \lambda/26$). These results are consistent with the hard-edge versus Gaussian mask lab experiments of Park et al. 2006, taking into consideration the differences in PSF structure and IWAs.

Curves showing contrast at the IWA and the relative improvement are shown in Figure 3 as a more continuous function of wavefront correction. Though Gaussian and 4th-order BL masks out-perform the hard-edge occulter at currently achievable Strehl ratios, they remain degenerate with one another into the realm of extreme AO. We next identify the conditions and parameters for which this performance degeneracy is broken.

---

[3]Notice that the IWA is rather loosely defined, and apodized masks can, in principle, work interior to the hard-edge mask. This benefit is likely difficult to exploit in practice, but constitutes an important caveat to the analysis. We assume that speckle-nulling is only applied exterior to the IWA.

4.2. Gaussian vs. Band-Limited Masks

In order to compare apodized masks to one another, consideration of the light distribution pattern in the Lyot pupil plane must be made. It is clear from the previous section that Gaussian masks are competitive with BL masks in terms of contrast even at very high Strehl ratios. Thus, we can use the Lyot plane patterns shown in the third column of Table 1 for qualitative guidance.

Consider the effect of changing the Lyot stop diameter, D_L, for each of the apodized masks. With small non-zero stop sizes, the contrast at a given location on the detector is governed by the competing effects of speckle noise intensity and the achievable peak intensity of an off-axis source. The speckle noise intensity scales as D_L^2, whereas the companion peak intensity, $\hat{I}(0)\,|M(r)|^2$, scales as D_L^4. The result is a net improvement in contrast and the apodized masks perform comparably, until D_L grows large enough to leak significant levels of diffracted starlight.

As the Lyot stop size increases further, the contrast generated by BL masks does not degrade in as smooth a fashion as the Gaussian mask, since the diffracted light is tightly concentrated into a small region that follows the contour of the telscope entrance aperture. Instead, the transition away from optimal performance is more abrupt. The width of the transition region in the Lyot plane narrows as the wave front correction improves, and the transition occurs at progressively smaller Lyot stop sizes for masks of higher-order (8th-, 12th-, ... etc.).

These effects are seen in Figure 4, where we plot contrast at the IWA against Lyot stop throughput for two levels of wavefront correction. At $\sim 90\%$ Strehl (rms WFE $= \lambda/20$), the apodized masks are clustered to within an order of unity in contrast from one another, but clearly out-perform the hard-edge occulter. At $\sim 96\%$ Strehl (rms WFE $= \lambda/30$), the apodized mask performance degeneracy is broken, and optimum Lyot stop sizes become more evident. In particular, the 4th-order band-limited mask affords an $\sim 10\%$ gain in Lyot stop throughput over the Gaussian mask (60% vs. 50%). The 8th-order and 12th-order masks generate slightly worse contrast and with $\lesssim 40\%$ and $\lesssim 15\%$ throughput respectively. These exact values depend upon the entrance aperture geometry, operating bandwidth, IWA, mask-function, and mask-type (linear, radial, or separable), but the trend is nevertheless the same at this level of wave front correction.

Generating Strehl ratios beyond 96% on large ground-based telescopes in the near future is rather unlikely.[4] Additional complications such as differential chromatic wavefront sensing

[4]The JWST however will provide a unique and stable platform for coronagraphy in the $3-5\,\mu$m band

and correction limitations and photon noise are significant at this level (Nakajima 2006, Guyon 2005). The potential benefits in using higher-order BL masks from the ground are thus restricted to guarding against low-order aberrations introduced downstream from the AO system, but at the expense of contrast, throughput, and angular resolution.

4.3. Tip/Tilt & Low-order Aberration Sensitivities

Thus far we have neglected quasi-static phase errors, or, at least, have assumed that the resulting scattered light has been judiciously removed with speckle-nulling hardware.[5] In this section we take a closer look at the issue. To get a feel for the problem, we calculate the contrast degradation due to just one error, systematic misalignment, at several characteristic levels of AO correction. Then we combine the results with theoretical low-order phase aberration information gathered from other studies and discuss the implications. This analysis along with that laid out in the previous two sections provides important first-order guidelines for selecting coronagraphic image masks for extreme AO systems.

Image mask response to quasi-static aberrations impacts the dynamic range and duty-cycle efficiency of high-contrast observations. For instance, in the case of tip/tilt errors, on-sky tracking latency or telescope-to-instrument flexure may lead to misalignments that leak significant amounts of light. Clearly, the masks presented here have different levels of resistance to such errors.

To assess pointing sensitivities, systematic tilt phase aberrations were added to the wavefront at the AO-coronagraph (IDL-MATLAB) interface. Optimum Lyot stop sizes were used for each mask, and median, instead of mean, intensities were evaluated to prevent bias towards poor contrast. The $1\,\lambda/D$ annulus directly outside the coronagraph IWA remained centered on the star as it was methodically shifted relative to the mask. Results are shown in Fig. 5 for linear alignment errors up to $5\,\lambda/D$.

At relatively low Strehl ratios ($\lesssim 88\%$), hard-edge masks perform comparably with apodized masks provided that the pointing error does not exceed $\sim 2\ \lambda/D$. At higher levels of correction ($\gtrsim 88\%$), mask alignment becomes more critical. In this regime, apodized masks are capable of generating significantly deeper contrast than the hard-edge mask. In particular, the Gaussian and 4th-order BL masks provide optimum contrast when aligned to

---

from space (Green et al. 2005).

[5]Actually the light must go somewhere in order to conserve energy. It is sometimes preferable to simply place it on the other side of the image plane during a given integration.

better than $\sim 1\,\lambda/D$ at $\sim 88\%$ Strehl and $\sim 0.5\,\lambda/D$ at $\sim 94\%$ Strehl. If such accuracy is difficult to manage, higher-order BL masks may be chosen over the Gaussian and 4th-order BL mask, with the usual tradeoffs (§4.2).

This analysis is also applicable to low-order aberrations in a more general sense. Shaklan & Green 2005 have shown that the 'order' of the mask (4th, 8th, 12th, ... etc.) uniquely determines a coronagraph's sensitivity to aberrations (tip/tilt, focus, astigmatism, coma, trefoil, spherical, ... etc.). The result is that higher-order masks, which are intrinsically broader, are naturally better filters of any given low-spatial-frequency phase error. For example, expansion of Equ. 2 shows that the Gaussian mask intensity transmission profile near the optical axis depends on r raised to the fourth power; thus, it is a 4th-order mask (Fig. 1). Figure 5 confirms that the Gaussian mask follows the 4th-order BL mask tilt sensitivity curve, and that higher-order BL masks follow suit.

The hard-edge mask may be considered in the limit as the exponent of the intensity transmission approaches infinity. It is effectively a mask of infinite order, and thus the most resistant to low-spatial-frequency aberration content. The sharp boundaries of the hard-edge mask however also make the coronagraph leak the most starlight. Combining this information, we recognize that Fig. 5 is qualitatively illustrative of a trend applicable to all individual phase aberrations, and sums of (orthogonal) phase aberrations, introduced downstream from the AO DM and wavefront sensor. As the phase errors increase, the contrast generated by apodized masks will rise (degrade) from the AO noise floor and eventually intersect the hard-edge mask curve.

In general, quasi-static phase errors further reduce the Strehl ratio. Therefore the situation is slightly more complicated than with tip/tilt alone, which, strictly speaking, is a change to the pointing vector and not an aberration. Nevertheless, we can extend the principle to quantitatively include them all.

Consider the final measured Strehl ratio, S, written as a decomposition of uncorrelated errors (Sandler et al. 1994):

$$S = S_1\, S_2\, S_3\, ...\, S_n, \tag{7}$$

where each S_i with $1 \leq i \leq n$ represents an independent Strehl degradation. An equivalent statement is that uncorrelated wavefront errors add in quadrature. Since the Strehl ratio produced by the AO system is unrelated to the subsequent optical path, we let $S = S_{AO}\, S_{qs}$ describe the final stellar image, where S_{AO} is the AO-corrected Strehl ratio (as has been used throughout the text and figures) and S_{qs} is the Strehl ratio due to *all* quasi-static phase aberrations introduced downstream from the AO DM and wavefront sensor.

Results from §4.1 and Fig. 5 show that use of an apodized mask, preferably the 4th-

order BL mask (§4.2), is justified only when $S_{AO} \gtrsim 88\%$. Thus, we require that the measured Strehl ratio satisfy the condition:

$$S \gtrsim 0.88\, S_{qs}, \tag{8}$$

where $0 \leq S_{qs} \leq 1$ is the intrinsic Strehl of the optical system. With an internal fiber-coupled source, such as a calibration lamp, S_{qs} can be measured when the AO DM is inactive and flat, so far as one might trust zeroing the actuator voltages. We note that this relationship is valid only in the high-Strehl regime ($\sigma \lesssim \lambda/2\pi$).

The effects of speckle-nulling can be incorporated by noticing that contrast curves such as those shown in Fig. 5, and similar graphs for the other phase errors present in a real system, will be "flattened" by the additional DMs (see §2). In other words, the extra degrees of freedom afforded with this hardware compensate for quasi-static aberrations whose spatial-frequencies match the intended search area. Long-lived speckles may be nulled to an intensity level where the contrast curves in Fig. 5 intersect the vertical axes; this is true for any such aberration. A candidate companion would then be noticed by the inability of the instrument to remove its mutually incoherent signal. Subsequent changes to the shape of the DMs and hence location of the dark hole might indicate the presence of other faint sources.

As an example, consider a measured Strehl ratio $S = 85\%$ with a system that has an intrinsic Strehl ratio $S_{qs} = 94\%$. According to Equ. 8, we are indeed justified in using the 4th-order BL mask for this application. However, if the additional DMs cannot remove quasi-static speckles from the region of interest down to the intensity of the AO-limited noise floor, we may consider switching to a higher-order mask, such as the 8th-order or 12th-order BL mask, to help filter stellar residuals before they illuminate the detector.

These results allow us to make rather strong conclusions regarding the implementation guidelines for image masks included in this study. We state them concisely in the next section. For further discussion of low-order phase aberrations within the context of Lyot coronagraphy, see Sivaramakrishnan et al. 2005, Lloyd & Sivaramakrishnan 2005, Shaklan & Green 2005, and Crepp et al. 2006.

5. Summary & Concluding Remarks

One should select an image mask whose rejection of starlight is commensurate with the noise floor set by the AO system. Our numerical simulations imply the following:

(1) Apodized masks should replace the hard-edge mask only when on-sky Strehl ratios, S, exceed $\sim 0.88\, S_{qs}$, where S_{qs} is the Strehl ratio due to all quasi-static phase aberrations

introduced by the instrument, downstream from the AO DM. Below this level of correction, the hard-edge mask outperforms apodized masks, not by reaching deeper levels of contrast, but by generating similar contrast (§4.1) and throughput (§4.2) with more resistance to quasi-static errors. This result is independent of entrance aperture geometry and bandpass.

(2) Since 4th-order BL masks yield more Lyot stop throughput than the Gaussian mask, and apodized masks with smooth intensity transmission gradients are equally difficult to manufacture, Gaussian masks should not be implemented under any foreseeable conditions on telescopes with uniform transmission entrance apertures.

(3) The selection of higher-order BL masks over the 4th-order BL mask is relegated to situations where both the ability to correct for the atmosphere to a very high degree and the inability to adequately null quasi-static speckles is simultaneously present.

For the operating range often considered with a traditional Lyot coronagraph, IWA $= 3 - 5\ \lambda_{max}/D$, the exact contrast and throughput values will deviate from those reported in §4, but in a rather predictable manner. The italicized conclusions however do not change with these considerations. It is also important to mention that Strehl ratios can be somewhat pesky to calculate in practice. Experimentally determined values are accurate only to several percent if the image is not spatially sampled at a rate higher than twice the Nyquist frequency (Roberts et al. 2004).

The hard-edge occulting mask is a remarkably relevant coronagraphic tool in an age of sophisticated wavefront correction techniques and clever applications of Fourier optics. Apodized masks, or binary versions of apodized masks (Kuchner & Spergel 2003), require nano-fabrication capabilities at visible and near-IR wavelengths (Balasubramanian et al. 2006, Crepp et al. 2006, Carson et al. 2005b, Debes et al. 2004, Trauger et al. 2004); this can be a strong deterrent and should be avoided unless Equ. 8 is satisfied (although, in a fast optical system, the focal ratio may impose stringent tolerances when building a hard-edge mask as well). In the realm of extreme AO, the 4th-order BL mask should be implemented, so long as quasi-static phase aberrations are manageable with speckle-nulling hardware.

Finally, our calculations suggest that the wavefront correction levels required for ground-based observations preclude reliable spectroscopic measurements of close-separation companions that are more than approximately one million times dimmer than their host star. Presumably, space-based instruments will be able to do much better. Nevertheless, this result is still more than an order of magnitude deeper than current AO-coronagraphs provide.

The authors are grateful to Joseph Carson for his guidance in AO simulation code

development and the anonymous referee for helpful comments that improved the paper. This work was partially supported by NASA with grants NNG06GC49G, NNG05G321G and NNG05GR41G, the NSF with grants NSF AST04-51407 and AST04-51408, the TPF program, the UCF-UF SRI program, and the University of Florida. JC acknowledges support from the SPIE and a Grant-In-Aid-of-Research from the National Academy of Sciences, Administered by Sigma Xi, The Scientific Research Society.

REFERENCES

Abe, L., Murakami, N., Nishikawa, J., & Tamura, M. 2006, A&A, 451, 363

Absil, O., den Hartog, R., Gondoin, P., Fabry, P., Wilhelm, R., Gitton, P., & Puech, F. 2006, A&A, 448, 787

Aime, C. 2005, A&A, 434, 785

Balasubramanian, K., et al. 2006, IAU Colloq. 200: Direct Imaging of Exoplanets: Science & Techniques, 405

Biller, B. A., Kasper, M., Close, L. M., Brandner, W., & Kellner, S. 2006, ApJ, 641, L141

Brunetto, E. T., Dierickx, P., Gilmozzi, R., Le Louarn, M., Koch, F., Noethe, L., Vérinaud, C., & Yaitskova, N. 2004, Proc. SPIE, 5382, 159

Carson, J. C., Eikenberry, S. S., Brandl, B. R., Wilson, J. C., & Hayward, T. L. 2005a, AJ, 130, 1212

Carson, J. C., Wilson, D. W., & Trauger, J. T. 2005b, Proc. SPIE, 5905, 427

Chauvin, G., Lagrange, A.-M., Dumas, C., Zuckerman, B., Mouillet, D., Song, I., Beuzit, J.-L., & Lowrance, P. 2004, A&A, 425, L29

Chauvin, G., et al. 2005, A&A, 438, L29

Close, L. M., et al. 2005, Nature, 433, 286

Crepp, J. R., Ge, J., Vanden Heuvel, A. D., Miller, S. P., & Kuchner, M. J. 2006, ApJ, 646, 1252

Debes, J. H., Ge, J., Kuchner, M. J., & Rogosky, M. 2004, ApJ, 608, 1095

Debes, J. H., Ge, J., & Chakraborty, A. 2002, ApJ, 572, L165

Ellerbroek, B., Britton, M., Dekany, R., Gavel, D., Herriot, G., Macintosh, B., & Stoesz, J. 2005, Proc. SPIE, 5903, 20

Green, J. J., Beichman, C., Basinger, S. A., Horner, S., Meyer, M., Redding, D. C., Rieke, M., & Trauger, J. T. 2005, Proc. SPIE, 5905, 185

Guyon, O. 2005, ApJ, 629, 592

Guyon, O., Pluzhnik, E. A., Kuchner, M. J., Collins, B., & Ridgway, S. T. 2006, ApJS, 167, 81

Hayward, T. L., Brandl, B., Pirger, B., Blacken, C., Gull, G. E., Schoenwald, J., & Houck, J. R. 2001, PASP, 113, 105

Itoh, Y., Oasa, Y., & Fukagawa, M., astro-ph/0608362

Lloyd, J. P., & Sivaramakrishnan, A. 2005, ApJ, 621, 1153

Lyot, B. 1939, MNRAS, 99, 580

Kasdin, N.J., Vanderbei, R.J., Spergel, D.N., Littman, M.G. 2003, ApJ, 582, 1147

Kuchner, M.J. & Traub, W.A. 2002, ApJ, 570, 900

Kuchner, M.J., Crepp, J., & Ge, J. 2005, ApJ, 628, 466

Macintosh, B. A., et al. 2006, Proc. SPIE, 6272,

Macintosh, B. A., et al. 2003, Proc. SPIE, 5170, 272

Makidon, R. B., Sivaramakrishnan, A., Perrin, M. D., Roberts, L. C., Jr., Oppenheimer, B. R., Soummer, R., & Graham, J. R. 2005, PASP, 117, 831

Marois, C., Doyon, R., Nadeau, D., Racine, R., Riopel, M., Vallée, P., & Lafrenière, D. 2005, PASP, 117, 745

Marois, C., Lafrenière, D., Doyon, R., Macintosh, B., & Nadeau, D. 2006, ApJ, 641, 556

Metchev, S. A., & Hillenbrand, L. A. 2004, ApJ, 617, 1330

Lloyd, J.P. & Sivaramakrishnan, A. 2005, ApJ, 621, 1153

Mawet, D., Riaud, P., Absil, O., & Surdej, J. 2005, ApJ, 633, 1191

Mayama, S., et al. 2006, PASJ, 58, 375

Murakami, N., & Baba, N. 2005, PASP, 117, 295

Nakajima, T., astro-ph/0608388

Neuhäuser, R., Guenther, E. W., Wuchterl, G., Mugrauer, M., Bedalov, A., & Hauschildt, P. H. 2005, A&A, 435, L13

Oppenheimer, B. R., et al. 2004, Proc. SPIE, 5490, 433

Park, R., Close, L. M., Siegler, N., Nielsen, E. L., & Stalcup, T. 2006, PASP, 118, 1591

Racine, R., Walker, G. A. H., Nadeau, D., Doyon, R., & Marois, C. 1999, PASP, 111, 587

Roberts, L. C., Jr., et al. 2004, Proc. SPIE, 5490, 504

Roddier, F., Roddier, C. 1997, PASP, 109, 815

Rouan, D., Riaud, P., Boccaletti, A., Clénet, Y., & Labeyrie, A. 2000, PASP, 112, 1479

Sandler, D., Stahl, S., Angel, J.R.P., Lloyd-Hart, M., & McCarthy, D., 1994, J. Opt. Soc. Am., 11, 925

Serabyn, E., et al. 2005, Proc. SPIE, 5905, 272

Serabyn, E., Wallace, K., Troy, M., Mennesson, B., Haguenauer, P., Gappinger, R., & Burruss, R., astro-ph/0702592, accepted to ApJ

Shaklan, S.B., & Green, J.J. 2005, ApJ, 628, 474

Sivaramakrishnan, A., Koresko, C.D., Makidon, R.B., Berkefeld,T., & Kuchner, M.J. 2001, ApJ, 552, 397

Sivaramakrishnan, A., & Yaitskova, N. 2005, ApJ, 626, L65

Sivaramakrishnan, A., & Lloyd, J. P. 2005, ApJ, 633, 528

Soummer, R. 2005, ApJ, 618, L161

Trauger et al., 2004, Proc. SPIE, 5487, 1330

Troy, M., Dekany, R., Brack, G., Oppenheimer, B., Bloemhof, E., Trinh, T., Dekens, F., Shi, F., Hayward, T., & Brandl, B. 2000, Proc. SPIE, 4007, 31

Troy, M., Crossfield, I., Chanan, G., Dumont, P., Green, J. J., & Macintosh, B. 2006, Proc. SPIE, 6272,

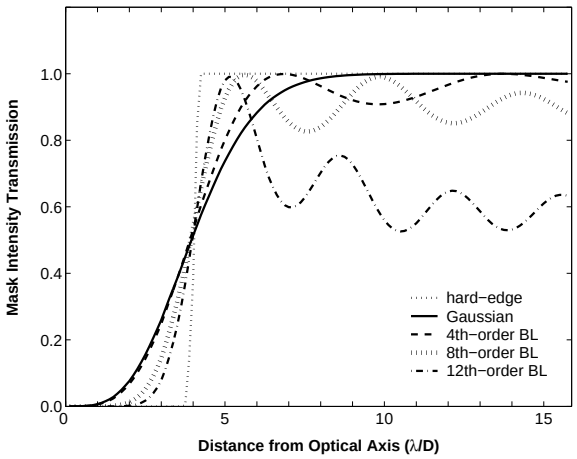

Fig. 1.— Intensity transmission profiles for each of the radial image masks. The IWA = 4 λ/D. Band-limited (BL) masks have extended off-axis attenuation, which allows them to be composed of a finite range of low spatial-frequencies. This feature offers unlimited dynamic range as the Strehl ratio approaches 100%. A Lyot-style coronagraph equipped with a BL mask is one of the leading candidate designs for the Terrestrial Planet Finder Coronagraph (*TPF-C*) space mission (Ford et al. 2004).

	Mask	Star×Mask	Lyot Plane	Final Image
Hard-Edge		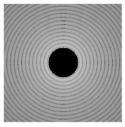		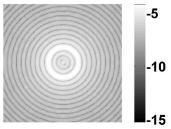
Gaussian		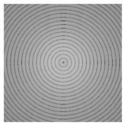	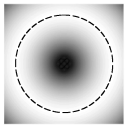	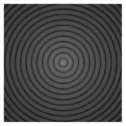
4th-order	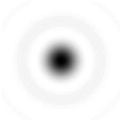	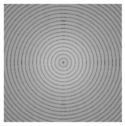	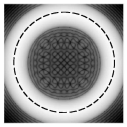	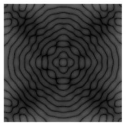
8th-order	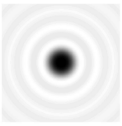	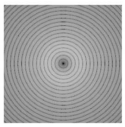	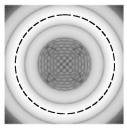	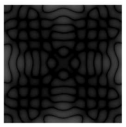
12th-order		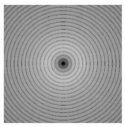	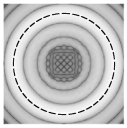	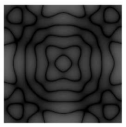

Table 1: Coronagraph simulations with perfect incident wavefronts. Intensities in the first two columns are shown on the same logarithmic scale using the mask profiles, $0 \leq |M(r)|^2 \leq 1$, in Fig. 1 and a normalized Airy pattern. The spatial extent of the image planes are identical and can be estimated from knowing that the hard-edge mask has a diameter of 8 λ/D. A dashed line in the 'Lyot Plane' column indicates the outline of the circular unobstructed entrance aperture. An ∼60% throughput Lyot stop was used for the hard-edge, Gaussian, and 4th-order BL masks. The 8th-order and 12th-order BL masks offer better rejection of low-order aberrations at a cost of throughput and angular resolution. The 'Final Image' column shows the contrast generated by each mask using the logarithmic scale in the hard-edge mask row; BL masks remove on-axis starlight down to the numerical noise level of the simulations ($< 10^{-12}$).

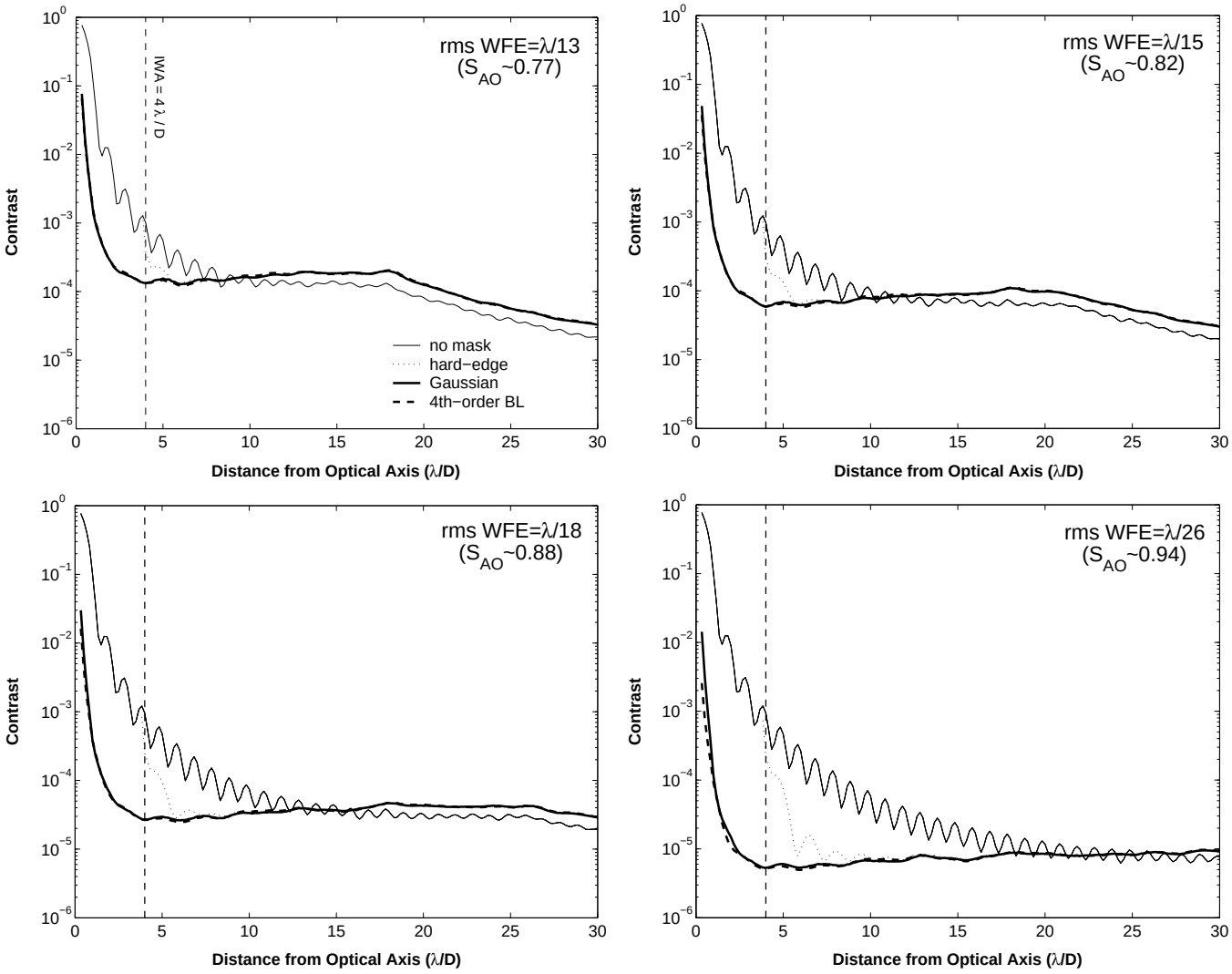

Fig. 2.— Azimuthally averaged contrast curves for the hard-edge, Gaussian, and 4th-order BL image masks using a fixed circular Lyot stop size with ∼60% throughput. The Lyot stop for the Airy pattern has 100% throughput.

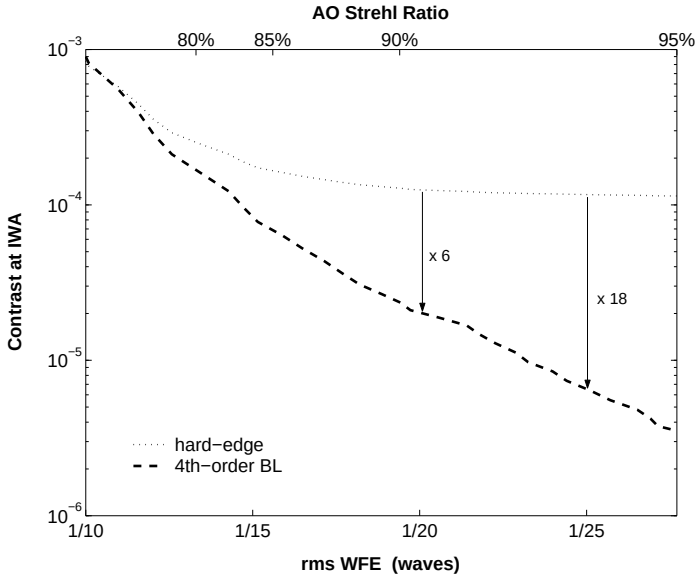

Fig. 3.— Average contrast within the $1\,\lambda/D$ wide annulus directly outside of the coronagraph IWA as a continuous function of atmospheric wavefront correction and the relative gain (shown by arrows) achieved by switching to the 4th-order BL mask. The hard-edge mask's performance is limited by starlight diffracted into the interior of the $\sim 60\%$ throughput Lyot stop. This prevents significant improvements beyond $\sim 88\%$ Strehl.

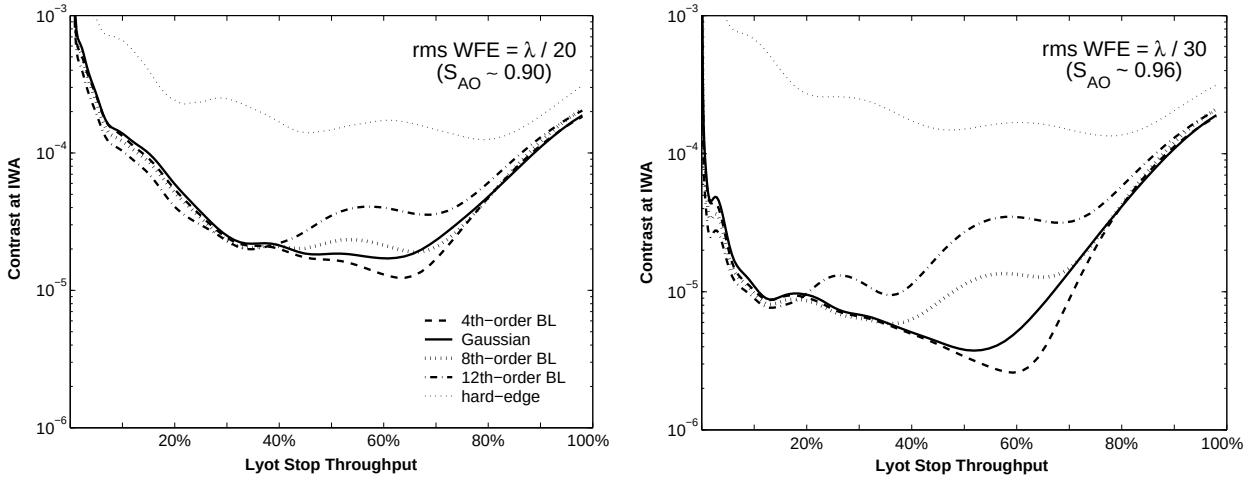

Fig. 4.— Average contrast within the $1\,\lambda/D$ wide annulus directly outside the coronagraph IWA as a function of Lyot stop throughput for $\sim 90\%$ Strehl (left) and $\sim 96\%$ Strehl (right).

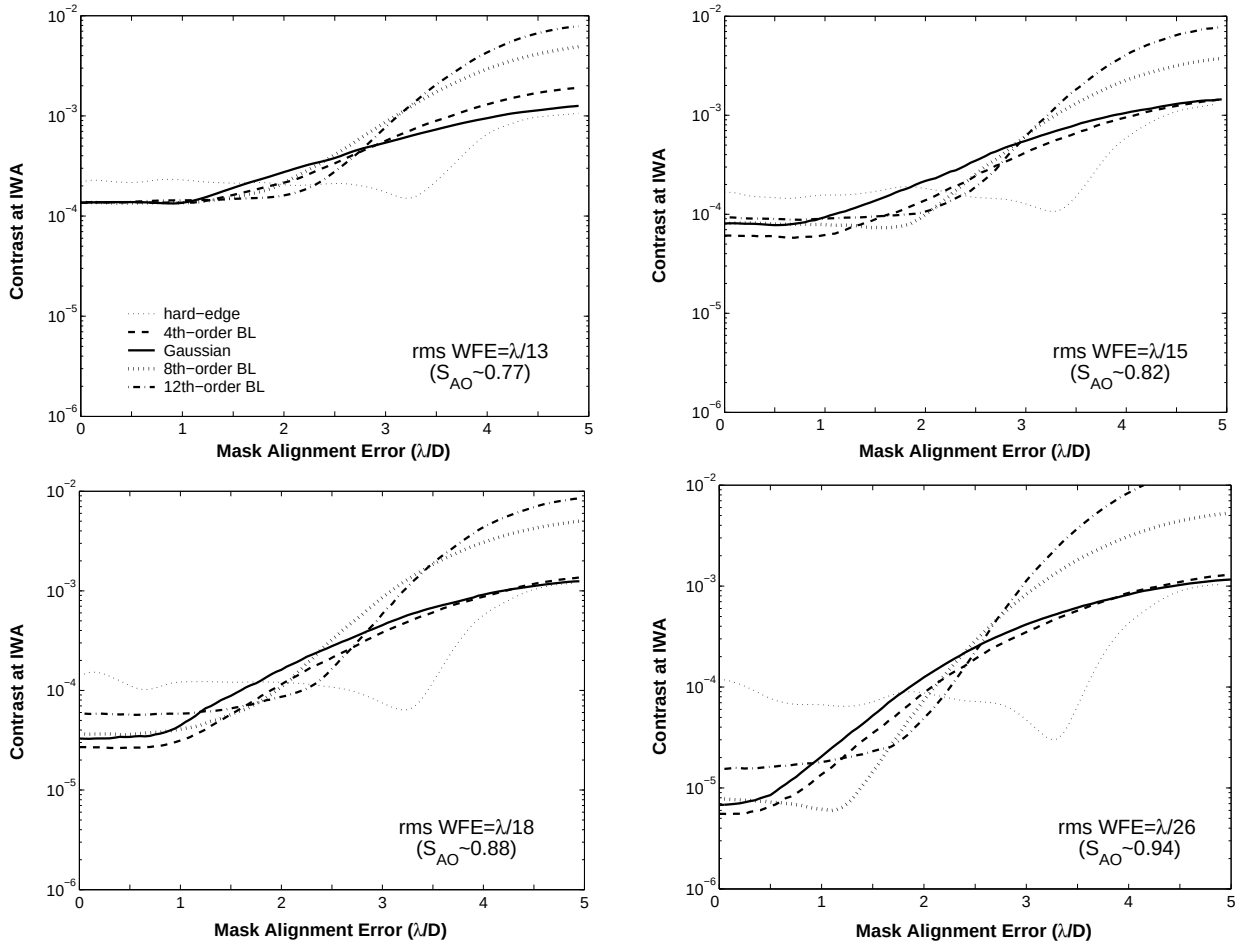

Fig. 5.— Median contrast within the $1\,\lambda/D$ annulus outside the coronagraph IWA as a function of systematic tilt error for several characteristic levels of wavefront correction using optimal Lyot stop sizes. Note that the Gaussian mask is a 4th-order mask. The non-monotonic changes in contrast are a result of calculating the median intensity with alignment errors in a circular geometry and phasing between the Airy pattern and the mask intensity transmission (see Lloyd & Sivaramakrishnan 2005).